PALEOCEANOGRAPHY, VOL. 8, NO. 1, PAGES 7-21, FEBRUARY 1993

WHAT CONTROLS OPAL PRESERVATION IN TROPICAL DEEP-SEA SEDIMENTS?

D. Archer, M. Lyle, K. Rodgers, and P. Froelich

Abstract. Measurements of opal preservation in deep sea sediment cores have been presented in three ways: the opal concentration as a fraction of total dry weight ($\%opal_{tot}$), the opal concentration normalized to calcite-free dry weight ($\%opal_{calcite\text{-}free}$), and the opal accumulation rate (opal MAR). It is tempting to interpret changes in these indices as indicators of rates of biological production in past oceans. Based on theoretical constraints, we argue that in typical tropical and subtropical sediments, both $\%Opal_{calcite\text{-}free}$ and opal MAR reflect a significant artifact of dilution by other phases. Thus the band of high $\%Opal_{calcite\text{-}free}$ in the equatorial Pacific appears to be caused in large part by the high %Calcite in that region, rather than by high opal productivity. The best candidate for a reliable paleoproductivity proxy appears to be $\%Opal_{tot}$. Unfortunately, present-day $\%Opal_{tot}$ data from tropical and subtropical regions show little or no systematic trend with the rain rate of opal. Pore water silica concentration data reveal that the apparent pore water opal solubility is not constant but correlates regionally with the rain rate of opal to the seafloor. A model that treats opal as a single homogeneous phase with a single well-defined solubility product predicts a strong dependence of opal concentration on rain rate (in stark contrast to the data), and a constant asymptotic pore water Si. Two models representing opal as multiple heterogeneous phases with different solubilities are able to reproduce the observed asymptotic pore water Si / rain rate relationship, but not the lack of rain rate trend in the opal concentration data. Only by assuming a systematic trend in the quality of opal (i.e., the solubility) as a function of opal production, can we reproduce the observed pattern of opal preservation. The implication of this study is that changes in opal preservation in the geologic record cannot simply be interpreted in terms of changes in surface ocean productivity until our understanding of opal diagenesis can be improved.

[1]Currently at Department of Geosciences, Boise State University, Idaho.

Paper number 92PA02803.
0883-8305/93/92PA-02803 $10.00

1. INTRODUCTION

Amorphous silica, or opal, is produced by diatoms, silicoflagellates, and radiolarians in the upper ocean. In spite of the thermodynamic tendency for biogenic opal to dissolve in sea water, opal is one of the three main constituents in deep-sea sediments (along with calcite and the products of terrestrial weathering). The preservation of opal in sediments is therefore controlled by competing kinetics of dissolution and removal from undersaturated sea water by burial. Because of this kinetic competition, sediments with high opal concentration tend to be found in regions of high opal productivity, such as in the southern ocean. In the tropics, surface sediments contain ~5-20% opal by weight.

The opal record in sediments is potentially useful as an indicator of past rates of primary production in the ocean, and of variations in the ecosystem of the surface ocean (for example, the dominance of calcitic versus siliceous plankton forms). Because the timing and frequency of opal preservation variations do not necessarily coincide with those of calcite or organic carbon, the opal record appears to contain independent information [Rea et al., 1991; Lyle et al., 1988]. In several cores, calcite preservation changes followed a beat of 100 kyr, while opal followed a 23-kyr frequency [Lyle et al., 1988].

Thus a means of quantitative interpretation of opal preservation in terms of the factors that control it would be invaluable to understanding the carbon cycle of oceans in the past.

We attack the problem by exploring the behavior of a model of the solid and dissolved forms of opal, calcite, organic carbon, and inert material (clay) in surface sediments. The model results are compared with observed pore water, solid concentration and accumulation rate data. The governing equations and solution strategy of the model is presented in section 2. A database of solid and pore water sediment data is presented in section 3. In Section 4 we argue, based on analytical and numerical results, that the calcite-free opal concentration and the opal mass accumulation rate indices should both be affected by major artifacts of dilution by other materials (calcite and clay). In Section 5, the model opal preservation is compared with data. We find that the model predicts much higher concentration of opal than is observed under conditions of high opal rain, and speculate that part of the discrepancy may be due to inadequate treatment of the pore water chemistry. However, Section 6 describes two alternative, testable models of opal dissolution that are able to simulate the pore water data, but are still unable to explain the preservation pattern of solid opal. Finally, we show in Section 7 that the observed opal preservation pattern can be reproduced if we assume that the solubility of opal varies systematically with opal rain (production).

2. MODEL FORMULATION

The model presented here is based on the calcite diagenesis model presented by Archer [1991], extended to simulate the effects of bioturbation, advection, and reaction of solid opal, calcite, organic carbon, and clay in the sediment mixed layer. Solid and pore water concentration profiles are calculated using a relaxation method algorithm described by Archer [1990]. Full simultaneous solution of the coupled multicomponent solid / pore water system is accomplished by iteration between simpler individual parts.

Solid Equations

The distribution of solids in the sediment mixed layer is controlled by the processes of sediment mixing (bioturbation), advection (burial of sediment relative to the sediment water interface) and reaction. The formulation includes the effects of the porosity gradient near the sediment water interface. The diffusion coefficient is taken to be constant (150 $cm^2\ kyr^{-1}$) within the bioturbated zone (to 10 cm), and zero below. A generalized equation for a solid species is

$$\frac{\partial c}{\partial t} = 0 = \frac{D_B}{(1-\Phi)}\ \frac{\partial}{\partial z}\left((1-\Phi)\ \frac{\partial c}{\partial z}\right) - \frac{\partial}{\partial z}(w\ c)\ -\ R_c\ M_c\ \rho^{-1}\ \frac{1}{(1-\Phi)} \qquad (1a)$$

where c is the dry weight fraction (g species/g solid total) of a solid component in the sediment (the solids are calcite, opal, organic carbon, and clay), D_B is the sediment mixing coefficient ($cm^2\ kyr^{-1}$), w is the sediment burial rate as a function of depth (cm kyr^{-1}), R_c is the reaction rate (mol $cm^{-3}\ s^{-1}$, where volume is total sediment plus pore water), M_c is the molecular weight, ρ the density of solid material, and Φ the porosity. Because the advection rate w depends on all species of interest (opal, calcite, organic carbon, and clay), this term represents the coupling between the equations for each solid. We are interested in the steady state values of c(z) rather than the time dependence of the equations; therefore, the term $\partial c/\partial t$ is set to zero.

In many cases, it is possible to simplify a model of sedimentary solids by making informed assumptions about the behavior of the solid in the sediment mixed layer. For example, when the calcite concentration is high, its profile can be reasonably described as well mixed [Keir, 1984; Archer, 1991], simplifying the calculations immensely. The burial flux of organic carbon is generally a negligible fraction of the rain rate; in this case, the advective term can be neglected [Murray and Grundmanis, 1980]. There are areas in the ocean where one or the other of these approximations is reasonable for solid opal [see Boudreau, 1990]. However, we have chosen here to solve the fully general case for each solid, taking full account of the diffusive and advective terms in equation 1a.

The reaction rate for opal (mol $cm^{-3}\ s^{-1}$) is

$$R_{opal} = k_{op}\ \%Op\ M_{op}^{-1}\ \rho\ \Phi\ (1-\Phi) \cdot (Si_{sat} - Si)\ H(Si_{sat} - Si) \qquad (1b)$$

where %Op is the weight fraction of opal in the sediment (g opal/g total solids), k_{op} is the rate constant ($cm^3\ mol^{-1}\ s^{-1}$), and $[Si]_{sat}$ is the apparent saturation value for opal (mol cm^{-3}). The Heaviside function, H, is 0 if the solution is supersaturated, and 1 if undersaturated, preventing precipitation of opal from supersaturated solutions. For calcite,

$$R_{cal} = k_c\ \%Cal\ M_{cal}^{-1}\ \rho\ \Phi\ (1-\Phi) \cdot \left(1 - \frac{[CO_3]}{[CO_3]_{sat}}\right)^n H([CO_3]_{sat} - [CO_3]) \qquad (1c)$$

where k_c is a reaction rate constant (taken to be 1 day^{-1} after Archer et al. [1989]), %Cal is the dry weight fraction of calcite in the sediment, $[CO_3]_{sat}$ is the saturation $[CO_3]$ with respect to calcite, and n is a reaction order, taken to be 4.5 [Keir, 1980]. For organic carbon,

$$R_{org} = k_{org}\ \%Org\ M_{org}^{-1}\ \rho\ \Phi\ (1-\Phi)\ H([O_2]) \qquad (1d)$$

where k_{org} is a rate constant (parameterized as a linear function of organic carbon rain, following Emerson [1985]), %Org is the organic carbon dry weight fraction, and *H* is the Heaviside function, reflecting shutdown of oxic organic carbon degradation where O_2 is depleted. (We neglect suboxic and anoxic organic carbon degradation: see Archer, 1991). Clay is treated here as an unreactive phase, with a reaction rate of zero.

$$R_{clay} = 0 \qquad (1e)$$

When solids dissolve in the mixed layer, the burial rate, w, decreases with depth from a maximum at the sediment surface.

The function w(z) represents a fifth unknown in the system. A simultaneous solution for %Op(z), %Cal(z), %Org(z), %Clay(z), and w(z) can be calculated by iteration. The initial approximation is that

$$w(z) = \text{the total sediment mass rain rate} \tag{2a}$$

for all z. Using this approximation, the equations for each of the solids (equation (1a) are calculated independently, using a relaxation method [Archer, 1990]. Then, values for w(z) are recalculated as

$$w(z) = \text{mass rain rate} - \int_{z'=0}^{z'=z} \Sigma\, R_C\, M_C\, dz' \tag{2b}$$

where R_C are the solid reaction rates (equations (2a)-(2d)). Using the new approximation for w(z), the solid distributions (equations (1a)-1e)) are recalculated for a second iteration. As the system of equations converges, the concentrations of the masses sum to unity,

$$\%Op + \%Cal + \%Org + \%Clay = 1 \tag{3}$$

The boundary conditions to the solid system equations are that the flux at the sediment surface is equal to the rain rate, as

$$(1 - \Phi)\, D_B \left.\frac{\partial c}{\partial z}\right|_0 - w(0)\, c = Rain_c \tag{4a}$$

where the rain rate of a component c is estimated from sediment trap data (see following). The boundary condition at the bottom of the bioturbated zone in the sediment is that the gradient with depth is equal to zero

$$\left.\frac{\partial c}{\partial z}\right|_{10\ cm} = 0 \tag{4b}$$

where the depth of the bioturbated layer is taken to be 10 cm below the sediment surface.

Pore Water Equations

Each of the solid reaction rates represented by equations (1a)-(1e) and (2a)-(2c) depend on the concentration of a solute in the pore water solution. Thus the steady state pore water chemical profiles are required to find the steady state solid distributions in the sediment mixed layer. The model formulation includes the effects of nonconstant diffusion coefficient with depth, but neglects the effects of the diffusive sublayer.

Silica. The equation describing the dissolved silica concentration in sediment pore water is

$$\Phi \frac{\partial Si}{\partial t} = 0 = \frac{\partial}{\partial z}\left(\frac{D_{Si}}{F}\frac{\partial Si}{\partial z}\right) + R_{opal} \tag{5}$$

where D_{Si} is the free diffusion coefficient for silica, F is the sediment formation factor [Ullman and Aller, 1982], and R_{opal} is the reaction rate given by equation (1b).

Oxygen. The oxidation of organic carbon is taken to be first order with carbon concentration, and zero order in O_2, until oxygen is depleted. This formulation neglects suboxic and anoxic respiration, but this simplification should not affect the diagenesis of opal that we are concerned with here. The equation governing dissolved oxygen is

$$\Phi \frac{\partial O_2}{\partial t} = 0 = \frac{\partial}{\partial z}\left(\frac{D_{O_2}}{F}\frac{\partial O_2}{\partial z}\right) - \left(\frac{O}{C}\right) R_{org} \tag{6}$$

where Do_2 is the diffusion coefficient of dissolved oxygen, and (O/C) is the oxygen to carbon stoichiometry for organic carbon oxidation (taken to be equal to 1.3).

Calcite. The solute controlling the dissolution rate of calcite, $[CO_3^{=}]$, is buffered by the carbonate buffer system; hence the entire carbonate pH system must be modeled, rather than simply the concentration of a single species such as Si or O_2. Through the carbonate system, the dissolution of calcite is tied to the respiration of organic carbon [Emerson and Bender, 1981]. The most convenient representation of the diffusion/reaction system is based on the pore water carbonate alkalinity (defined as $[HCO_2^{-}] + 2\,[CO^{3=}]$) and total CO_2 (defined as $[CO_2] + [HCO_3^{-}] + [CO_3^{=}]$), with a third equation representing the requirement of pH equilibrium at all depth. For alkalinity, the equation is

$$\Phi \frac{\partial\, alk}{\partial t} = 0 = \frac{\partial}{\partial z}\left(\frac{D_{HCO_3}}{F}\frac{\partial HCO_3}{\partial z}\right) + 2\frac{\partial}{\partial z}\left(\frac{D_{CO_3}}{F}\frac{\partial CO_3}{\partial z}\right) + 2\,R_{cal} \tag{7a}$$

for total CO_2,

$$\Phi \frac{\partial\, \Sigma CO_2}{\partial t} = 0 = \frac{\partial}{\partial z}\left(\frac{D_{CO_2}}{F}\frac{\partial CO_2}{\partial z}\right) + \frac{\partial}{\partial z}\left(\frac{D_{HCO_3}}{F}\frac{\partial HCO_3}{\partial z}\right) + \frac{\partial}{\partial z}\left(\frac{D_{CO_3}}{F}\frac{\partial CO_3}{\partial z}\right) + R_{org} + R_{cal} \tag{7b}$$

and reflecting pH equilibrium,

$$\frac{[CO_2]\,[CO_3^{=}]}{[HCO_3^{-}]^2} = \frac{K_1'}{K_2'} \tag{7c}$$

where D_X is the diffusion coefficient of solute x.

Because the dissolution of calcite is a strong function of pressure (depth) in the ocean, a test for the calcite preservation model was the behavior of calcite in sediment as a function of depth (the calcite lysocline) [Archer, 1991]. The value of the dissolution rate constant for calcite required to reproduce the calcite lysocline was consistent with microelectrode data [Archer et al., 1989]; the sediment rain and accumulation rates were also consistent with available data. The treatment of

calcite dissolution in the present work is based on FORTRAN code given by Archer [1990].

The boundary conditions for all pore water species are

$$C_{z=0} = C(\text{bottom water}) \quad (8a)$$

and

$$\left(\frac{\partial C}{\partial z}\right)_{z=10\text{ cm}} = 0 \quad (8b)$$

where C is a concentration of any pore water solute. For O_2, when oxygen is entirely consumed within the oxic zone, there is one value for the depth of oxygen penetration, z_{O2}, for which the organic carbon oxidation rate balances the diffusive oxygen flux across the sediment water interface; this depth is determined [Boudreau and Westrich, 1984; Archer and Devol, 1992] such that

$$\left(\frac{\partial C}{\partial z}\right)_{z=zo2} = 0 \quad (8c)$$

The depth of oxygen penetration, z_{O2}, is found by iteration (described below).

Coupled Solid / Solute System

A simultaneous solution for the solid / pore water system can be found by successive approximation. Beginning with an arbitrary initial guess at the solid concentrations, the oxygen and silica systems are each solved independently. The concentrations of the carbonate species (CO_2, HCO_3^-, and $CO_3^=$) are found simultaneously [Archer, 1991]. Using these pore water chemical solutions, the reaction rates of the solid species can be calculated and the solid equations solved. Since adjusting the solid concentrations changes the pore water reaction rates, the pore water and solid equations are solved in turn until the system converges.

3. AN OCEANOGRAPHIC DATASET

Sediment Rain and Accumulation

We will make use of a data base from the literature of locations in the ocean where rain rates of opal, calcite, and organic carbon have been measured using sediment traps, and where sediment composition and accumulation data are available (Table 1). Much of this data was presented by Dymond and Lyle [1993].

Dymond and Lyle [1993] present a compelling correlation between the fraction of the opal rain that is buried and the opal rain rate, which we reproduce in Figure 1a. However, based on theoretical arguments to come, we will argue that the observed opal accumulation is instead controlled by the total mass accumulation rate (Figure 1b). We also show opal concentration from the data set, as total and calcite-free, plotted against the opal rain (Figures 1c and 1d).

TABLE 1. The full data set of near-bottom sediment trap fluxes and sediment composition and accumulation rates

Site	Refe-rence	Depth	Lati-tude	Longi-tude	Cal. Rain	Org Rain	Op Rain	ΔCO_3	%Op	%Cal	MAR	%Op Pres
Atlantic												
HAP	1	5400	32.73	70.82	11	6	3		3	21	4.5	72
NAP	1	5847	23.20	63.98	5	4	2	-30	0	6	0.65	1
E	2	5068	13.50	54.00	8	5	4	7.9	2	28		
Pacific												
MFZ	1	4230	39.49	127.69	7	11	15	-10	3	2	3.24	11
ER	1	2200	47.97	128.10	12	9	12		9	46		
NS	1	2829	42.09	125.77	15	44	80		10	9	9.69	20
MW	1	2830	42.19	127.58	9	14	28	-10	6	1	4.01	14
G	1	3664	41.55	132.00	4	5	6		3	25	0.47	4
H	1	3565	6.57	92.77	13	7	6	-10	15	1	0.11	4
M	1	3150	8.83	103.98	7	12	12	-10	11	15	0.28	4
S	1	4620	11.06	140.14	5	3	6	-15	16	1	0.03	1
C	1	4445	1.04	138.94	21	11	18	-15	13	75	0.84	10
P1	2	5582	15.33	151.48	2	2	1	-40	0	9		
PB	2	3856	5.33	81.85	44	31	18	-10	7	22		

Units of depth are meters; rain rates are μmol cm^{-2} yr^{-1}; ΔCO_3 is the calcite saturation state in μM $CO_3^=$; %Op and %Cal are the dry weight fractions or opal and calcite; MAR is the total mass accumulation rate, in g kyr^{-1}, and %Op. Pres. is the calculated percentage of opal preservation. References: 1, Dymond and Lyle [1993]; 2, Honjo et al. [1982].

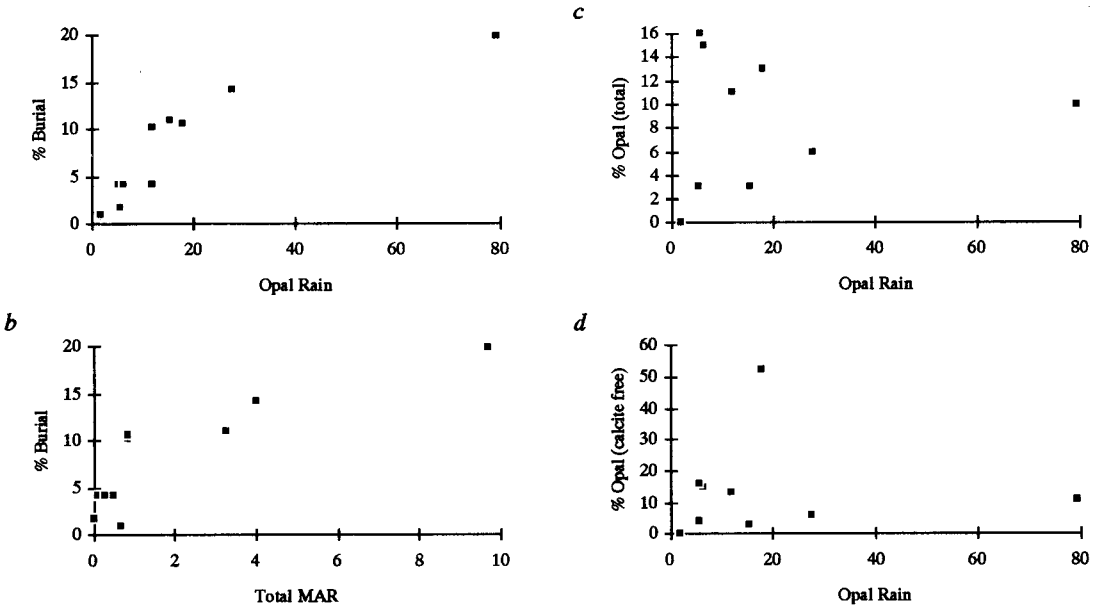

Fig. 1. (a) Scatterplot of the fraction of the opal rain that is buried against the opal rain rate to the seafloor (μmol cm^{-2} yr^{-1}), replotted from Dymond and Lyle [1993]. (b) Opal burial fraction against total MAR, units of g cm^{-2} yr^{-1}. (c) $\%Opal_{tot}$ (dry weight total fraction of opal in sediments) against opal rain, from Table 1. (d) $\%Opal_{calcite\text{-}free}$ against opal rain, from Table 1.

Pore Water Data

We have compiled published and unpublished pore water silica data (Figure 2). All of these data were taken after the importance of maintaining in situ core temperature during extraction was discovered [Fanning and Pilson, 1971]. Only locations for which the concentration of solid biogenic opal was reported, and is nonzero, are presented.

Oceanographers have long been puzzled by the observation that the asymptotic concentration of pore water silica with depth is lower than the laboratory measured solubility of acid cleaned biogenic opal or inorganically precipitated amorphous silica (~1000 μM at 4° C) [Hurd, 1973], in the presence of measurable amounts of biogenic solid opal. We shall see that this puzzle is central to understanding the preservation of solid opal in the geologic record.

Several hypothetical explanations for the apparent undersaturation of pore water silica were discussed by Hurd [1973]. One possibility is uptake of silica by some other solid phase, a "reverse weathering" reaction. However, the fact that opal is not entirely depleted after long exposure to the "undersaturated" pore water would require that the dissolution rate constant in the bottom half of the bioturbated zone must be 6-8 orders of magnitude lower than the value inferred from the pore water silica profile for the top half [Hurd, 1973]. No laboratory dissolution studies have noted changes in dissolution kinetics of this magnitude. Furthermore, it is difficult to conceive of a mechanism by which the asymptotic Si concentration should correlate with the opal rain rate, as observed. Accordingly, we regard this hypothesis as unsatisfactory.

An alternative hypothesis is that the solubility of sedimentary opal is lower than has been measured for pure amorphous silica. Lewin [1961] reported that the solubility of acid-cleaned diatoms cells was roughly a factor of five higher than for uncleaned, heat killed cells. Also, the presence of solid or dissolved alumina has been shown to lower the apparent solubility of amorphous silica [Lewin, 1961; Willey, 1975; Iler, 1973; van Bennekom et al., 1989, 1991]. A decrease in solubility also accompanies the transformation of amorphous silica to chrystobalite and quartz [Hurd and Theyer, 1975], although the time scales required for this process are too long to be relevant here.

Another clue to the mechanism of opal diagenesis is the observation that the asymptotic pore water Si correlates with the opal rain rate. By assuming that most of the rain of opal dissolves (burial represents 5-10% of rain: Figure 1a and 1b), we can calculate the rain rate from the diffusive flux of silica across the sediment water interface. Figure 3 shows this correlation. Recent pore water silica data from Martin et al. [1991] also reflect a rain rate trend, but only data from the top 5 cm of the pore water are reported: values less than the asymptotic Si. The trend observed here was also reported by Schink et al. [1974]. In the last section, we will suggest several mechanisms by which a sedimentary mixture of two or more opal fractions with differing solubilities could manifest itself as a correlation between asymptotic Si concentration and rain rate, as observed.

4. THE EFFECT OF DILUTION ON OPAL PRESERVATION

Because of the wide variation in calcite content of sediments associated with the calcite lysocline, opal concentration and downcore data are often presented normalized to a "calcite free" basis, as

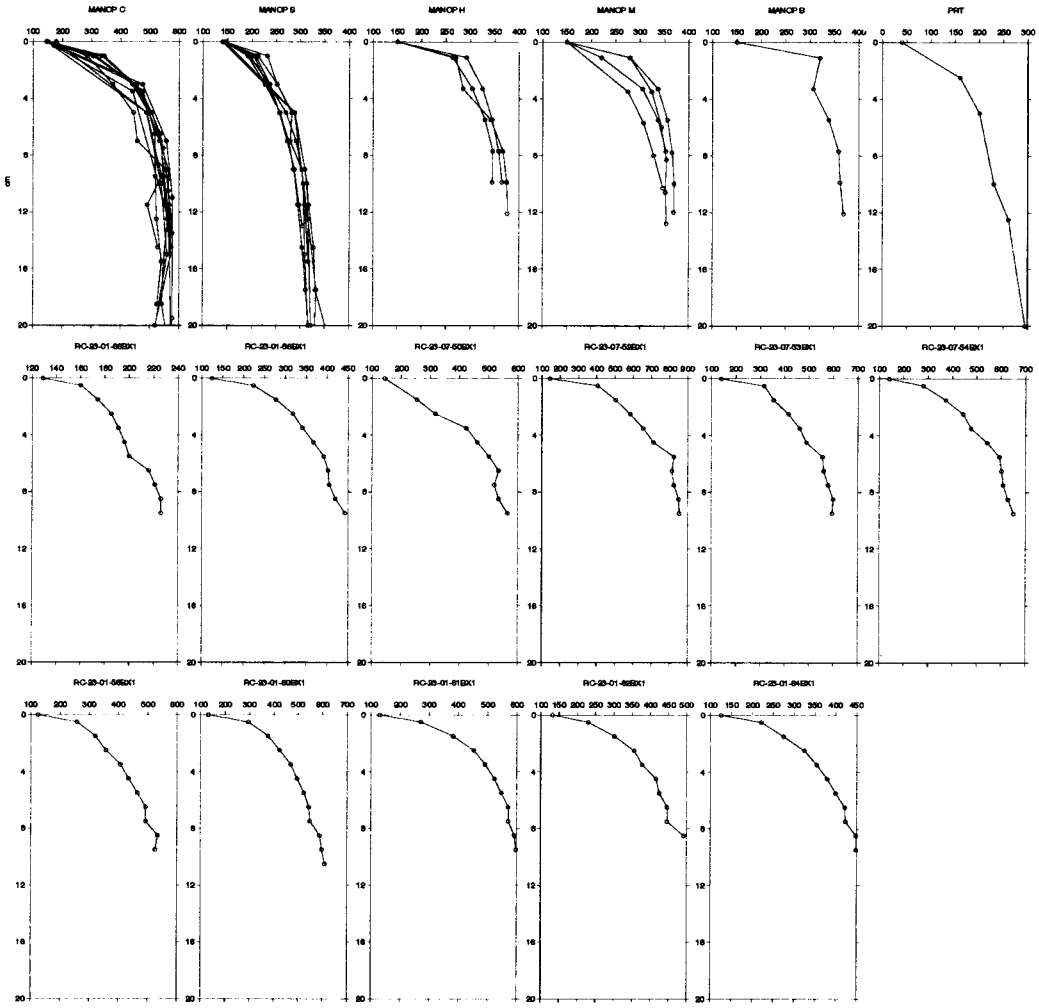

Fig. 2. A database of pore water silica data. Manop C and S data from Jahnke et al. [1982]: Manop M, B, and H data from Emerson et al. [1980]: PRT data is from the Puerto Rican Trench [Schink et al. 1975]. RC data is Froelich, unpublished, from the Equatorial Pacific: 50BX1; 1^{o} 1' N, 104^{o} 24' W, 3473m, 12.0% opal (total): 52BX1; 1^{o} 0' N, 118^{o} 12' W, 3857m, 12.7% opal: 53BX1; 0^{o} 59' N, 124^{o} 38' W, 4516m, 19.9% opal: 54BX1; 1^{o} 00' N, 133^{o} 41' W, 4212m, 11.6% opal: 56BX1; 3^{o} 58' S, 140^{o} 01' W, 4386m, 3.3% opal: 58BX1; 1^{o} 33' N, 140^{o} 00' W, 4211m, 7.7% opal: 60BX1; 00^{o} 29' N, 139^{o} 59' W, 4224m, 9.5% opal: 61BX1; 0^{o} 54' N, 140^{o} 02' W, 4328m, 13.3% opal: 62BX1; 2^{o} 00' N, 140,,01W, 4249m, 6.2% opal: 64BX1; 4.00N, 139^{o} 59' W, 4232m, 6.2% opal: 66BX1; 7^{o} 50' N, 140^{o} 00' W, 4939m, 14.7% opal.

$$\%Opal_{calcite\text{-}free} = \%Opal_{total} / (100 - \%Cal) \cdot 100\%$$

with the intention of correcting the opal signal for dilution by calcite. Our analysis suggests that this approach actually generates a calcite artifact in the opal signal, rather than removing it as intended. To explain why this is so, we make a few simplifying assumptions about the opal pore water and solid dynamics, that allow an analytical solution to the equations. We then illustrate the conclusions of the simplified system with the results of the full numerical solution.

To derive our simplified solution, we assume that the asymptotic pore water silica concentration is the saturation value. If we also make the approximations that the opal concentration, and the pore water diffusivity are constant with depth, we can integrate equation 5 to find that the pore water profile of dissolved silica in steady state is

$$Si(z) = Si_b + (Si_{sat} - Si_b) \cdot \exp\left(-\left(\frac{k\ \%Opal_{tot}\ M_{op}^{-1}\ \rho\ (1-\Phi)}{D_{Si/F}}\right)^{1/2} z\right) \qquad (9)$$

where Si_b is the bottom water value. The total rate of opal dissolution is balanced by the diffusive flux of silica into the overlying water, as

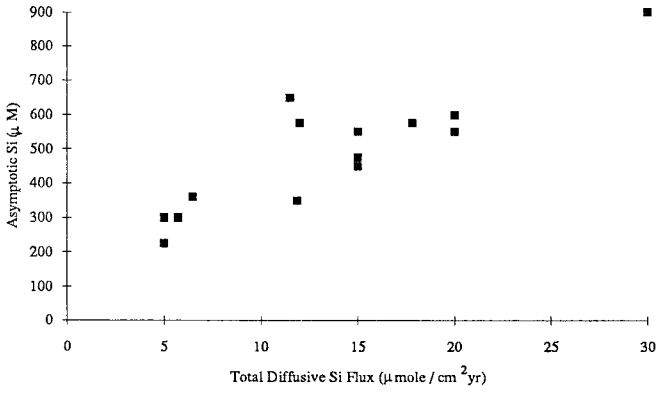

Fig. 3. Scatterplot of the observed asymptotic pore water concentration of silica from the data in Figure 2, against the diffusive flux of silica across the sediment water interface, calculated from the pore water profiles. Since burial only represents 5-10% of rain, we argue that the diffusive flux is a reasonable estimate of opal rain. The asymptotic Si values are all below the laboratory measured solubility of cleaned biogenic opal or inroganically precipitated amorphous silica (~ 1000 μM). Also, a clear correlation exists between the observed asymptotic silica concentration and the opal rain.

$$\Sigma Diss = \Phi \frac{D_{Si}}{F} \frac{\partial Si}{\partial z}(0) = \Phi \frac{D_{Si}}{F} (Si_{sat} - Si_b) \cdot \left(\frac{k \; \%Opal_{tot} \; M_{op}^{-1} \; \rho \; (1 - \Phi)}{D_{Si}/F} \right)^{1/2} \quad (10)$$

The pore water chemistry and the total dissolution rate are tied to the solid concentrations and the rain rate by the term $\%Opal_{tot}$ in this expression.

In steady state, we assume that the rain rate of opal to the seafloor is balanced by the depth-integrated sediment opal dissolution rate plus the burial rate. In much of the tropical and subtropical ocean, the burial term represents only ~10% of the rain rate (Figure 1), so that we can make the following approximation:

$$Rain \sim \Sigma Diss \quad (11)$$

Combining with (10) and solving for $\%Opal_{tot}$ we find

$$\%Opal_{tot} \sim \frac{Rain^2}{\Phi^2 \; D_{Si}/F \; (Si_{sat} - Si_b)^2 \; k \; M_{op}^{-1} \; \rho \; (1 - \Phi)} \quad (12)$$

or, in other words, we deduce that the concentration of opal in the sediment should scale as the rain rate of opal squared, under conditions where the saturation state and dissolution kinetics are constant.

The first observation that we draw from the above equation (12) for the opal concentration is that the rain and accumulation of other sedimentary constituents, for example calcite, do not appear, implying that the opal concentration is insensitive to dilution by other sedimentary components (this property is an implication of the assumption that Rain ~ ΣDiss). This prediction is illustrated by a model simulation of the calcite lysocline in Figure 4a, generated by keeping constant values of the rain rates and dissolution kinetics of all constituents, and varying the saturation state of the overlying water with respect to calcite. Even as increasing calcite dissolution (with depth in the water column) depletes calcite from 80% dry weight to negligible values, the steady state opal concentration is relatively constant. The reason for this behavior is implied by equations (11) and (12). When burial is insignificant, the rain rate must be balanced by dissolution. This externally specified dissolution flux must be supported by some particular concentration of opal in the zone of high dissolution near the sediment water interface. Under conditions of constant dissolution kinetics and overlying water chemistry, the dissolution rate depends only on the dry weight fraction of opal in the sediment. Hence the opal concentration, expressed as a fraction of total sediment, is driven toward the same steady state value regardless of dilution by calcite!

One implication of this behavior is that the $\%Opal_{calcite\text{-}free}$ should show a significant calcite artifact. That is to say, attempting to remove calcite concentration dependence by subtracting the calcite concentration actually makes the situation worse than simply presenting opal concentration as $\%Opal_{tot}$. The $\%Opal_{calcite\text{-}free}$ values from Figure 4a are presented in Figure 4b, to illustrate this point.

The idea may be relevant to opal preservation in the equatorial Pacific. Figure 5a and 5b show the %Calcite and $\%Opal_{calcite\text{-}free}$ in the eastern Equatorial Pacific, from Lyle [1992], with the familiar opal maximum near the equator (generally attributed to higher production and rain of opal to equatorial sediments). When the opal is presented as $\%Opal_{tot}$ (Figure 5c), the equatorial maximum disappears. This suggests that the $\%Opal_{calcite\text{-}free}$ maximum may be in part a reflection of the high %Calcite at the equatorial Pacific, which exist because of high calcite production and a local topographic high that coincides with the equator.

The accumulation rate of opal can be calculated as

$$Opal\ MAR = Total\ MAR * \%Opal_{tot} \quad (13)$$

and, if we decide based on equation (12) that $\%Opal_{tot}$ is held at a constant level by the required dissolution rate, then we conclude that the opal MAR should be linearly related to the burial rate of other solids, e.g., calcite. This can be seen in Figure 6. We conclude that interpretation of opal preservation data in terms of opal rain is complicated by changes in the burial rate of calcite and other diluting solids. Thus the use of opal MAR as an indicator of opal productivity is not supported by our analysis. On the basis of these results, we argue that the correlation between the opal preservation factor and the opal rain presented by Dymond and Lyle [1993], and reproduced here in Figure 1a, may be explained instead by variations in the total mass accumulation rate (Figure 1b).

We can illustrate this point by analogy to a strip-chart recorder, where the position of the pen represents $\%Opal_{tot}$ and sediment accumulates with movement of the chart paper. The opal accumulation rate is calculated as the area under the pen

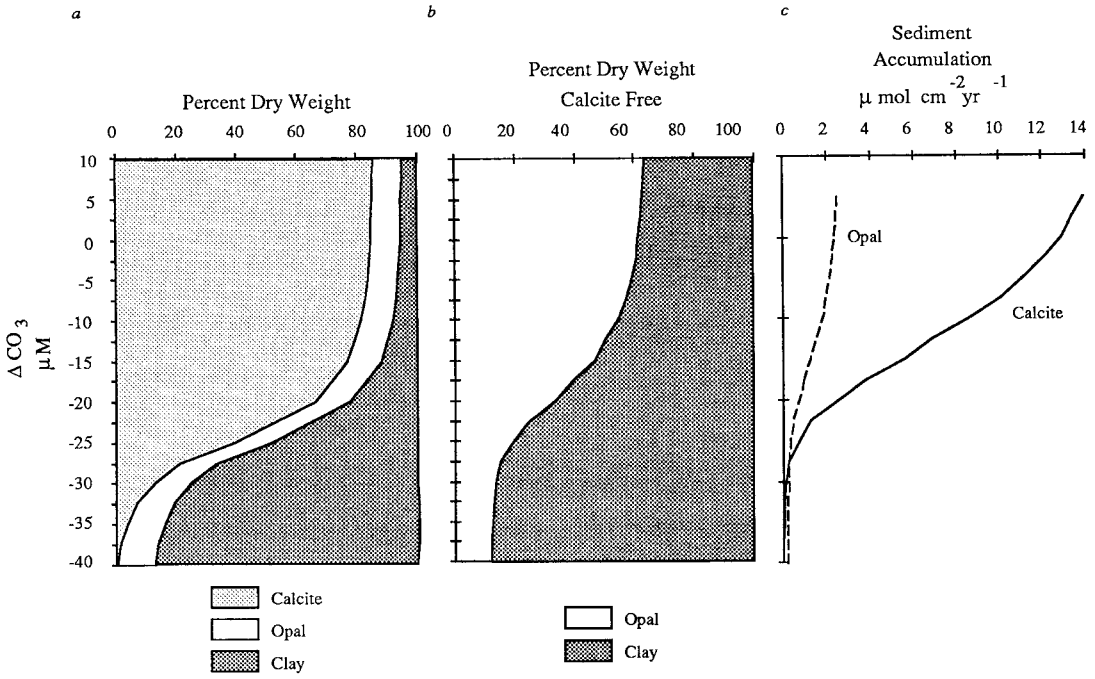

Fig. 4. A model of the behavior of opal across the calcite lysocline. Rain rate and dissolution kinetics are held constant in this simulation, except for the saturation state of calcite, which changes with pressure. Vertical axes represent the saturation state of the overlying water with respect to calcite, expressed as ΔCO_3 = $[CO_3]_{overlying\ water}$ - $[CO_3]_{saturation}$. Rain rates of calcite, opal, and organic carbon are 18, 15, and 14 μmol cm^{-2} yr^{-1}, respectively. Dissolution rate constants are 1 day^{-1}, 150 yr^{-1}, and (0.5 · $Rain_{org}$ [mol cm^{-2} yr^{-1}] × 10^{-3}) [s^{-1}], respectively. Solubility of opal is constant at 600 μM Si, and overlying Si was 150 μM. (a) An area plot representing a model simulation of the calcite lysocline. The steady state concentration of opal is relatively constant (~10%), in spite of dilution by calcite in the shallower sediments. See text for explanation. (b) Calcite-free opal concentrations, calculated from Figure 4a. The exercise demonstrates the artifact introduced into opal data when it is presented normalized to a calcite-free concentration. (c) Accumulation rate of calcite and opal across the model calcite lysocline. Opal accumulation shows a clear calcite artifact, implying that interpretation of opal accumulation in terms of opal productivity is not supported by our analysis.

curve on the paper, which depends on both the position of the pen and the speed of the paper. The crucial point is that in a correctly functioning strip-chart recorder, the position of the pen is independent of the speed of the paper. We argue that where burial represents a negligible fraction of the opal rain, as in most tropical and temperate ocean sediments, $\%Opal_{tot}$ is also relatively insensitive to the accumulation rate of other solid material. Thus opal accumulation ought to be correlated with changes in total sediment accumulation rate across the calcite lysocline.

This analogy can be contrasted with the "overworked leaf sorter" model described by Broecker and Peng [1982], in which a botanist attempts to selectively remove oak leaves as they land on a given plot on the forest floor. When the winds are high and lots of leaves fall on his plot, the botanist is overwhelmed and unable to keep pace with the leaf deluge, and some oak leaves escape his attention. The analogy applies to the case where the burial rate of opal is comparable to the dissolution rate, such as in southern ocean sediments.

In both cases, the opal accumulation rate increases with the burial rate of other material, but the mechanisms of action differ fundamentally. In the "strip chart recorder" analogy, appropriate to tropical and temperate ocean sediments, changes in total mass burial do not drive large relative changes in the opal dissolution rate, since a majority of the opal rain dissolves in any case. In contrast, in the southern ocean, represented by the Broecker and Peng analogy, burial does represent a significant fraction of the opal rain, and faster burial promotes opal preservation directly by competing kinetically with dissolution.

5. WHAT CONTROLS $\%Opal_{tot}$?

We have argued based on analytical and numerical results that of the three opal preservation indices in common use, $\%Opal_{tot}$, $\%Opal_{calcite\text{-}free}$, and opal MAR, only $\%Opal_{tot}$ has any hope of being a faithful recorder of the opal rain without artifacts of variations in concentration or burial of calcite and terrigenous material. Unfortunately, an examination of $\%Opal_{tot}$ plotted against opal rain in Figure 1c confounds this hope without any further analysis. Instead of a strong trend of $\%Opal_{tot}$ with opal rain, we see no trend, and

considerable scatter. It could be that the predicted trend exists in the real ocean but is obscured by uncertainty in the sediment trap data. Examination of the $\%Opal_{tot}$ distribution in the Eastern Equatorial Pacific (Figure 5c) reveals a slight equatorial maximum at 90°-100°E, but similar values can be found along 10°N in the subtropical gyre. The correlation between $\%Opal_{tot}$ and production, if it exists in the ocean, is certainly not as clear or reliable as has been supposed. We conclude, based on these observations, that there is at present little justification for interpreting regional or downcore variation in opal preservation in simple terms of opal production.

So what does control opal preservation in tropical sediments? It is clear that there exist significant regional variations in the $\%Opal_{tot}$ in deep-sea sediments (Figure 5c). Also, opal preservation recorded in cores apparently shows variation through time that is regionally coherent [Lyle et al., 1988]. It is intriguing that opal preservation tends to emphasize different Milankovich frequencies than does calcite preservation [Lyle et al., 1988: Rea et al., 1991]. Therefore understanding the factors that control opal preservation today must be a priority for paleoceanographers interested in the carbon cycle. The observed variations in $\%Opal_{tot}$, regionally or with time, correspond to the scatter in Figure 1c. As a prelude to understanding the scatter, we attempt to reproduce the first order behavior, namely the lack of trend between $\%Opal_{tot}$ and opal rain.

For each location in the sediment rain and solid composition data set (Table 1), we compare the model steady state $\%Opal_{tot}$ with data in Figure 6. The model is clearly overestimating the observed $\%Opal_{tot}$ at high opal rain, and underestimating the observations at low rain rates. Although the entire model-predicted field may scale higher or lower with changes in the model solubility product or dissolution kinetics, there is no way to change the model tendency to higher opal concentrations with higher opal rain.

Reexamination of equation (12) reveals the reason why. The equation states that, if the rate constant and kinetics for opal dissolution are held constant, then the concentration of opal (as a percent of total sediment) should scale with the rain rate to the second power. We can see this aspect of the model behavior more clearly in Figure 7. By using the values of the dissolution rate kinetics and saturation value from a given location, and the observed rain rates of calcite, opal, organic carbon, and clay, we simulate the steady state condition at two locations. From these starting points, the rain rates of opal are varied, while everything else is held constant. The model-predicted variation of %Opal with opal rain are depicted as curves labeled MANOP C and M, each of which begins with rain rate, solubility, and kinetics information inferred from MANOP data. MANOP site M, a low opal rain rate location,

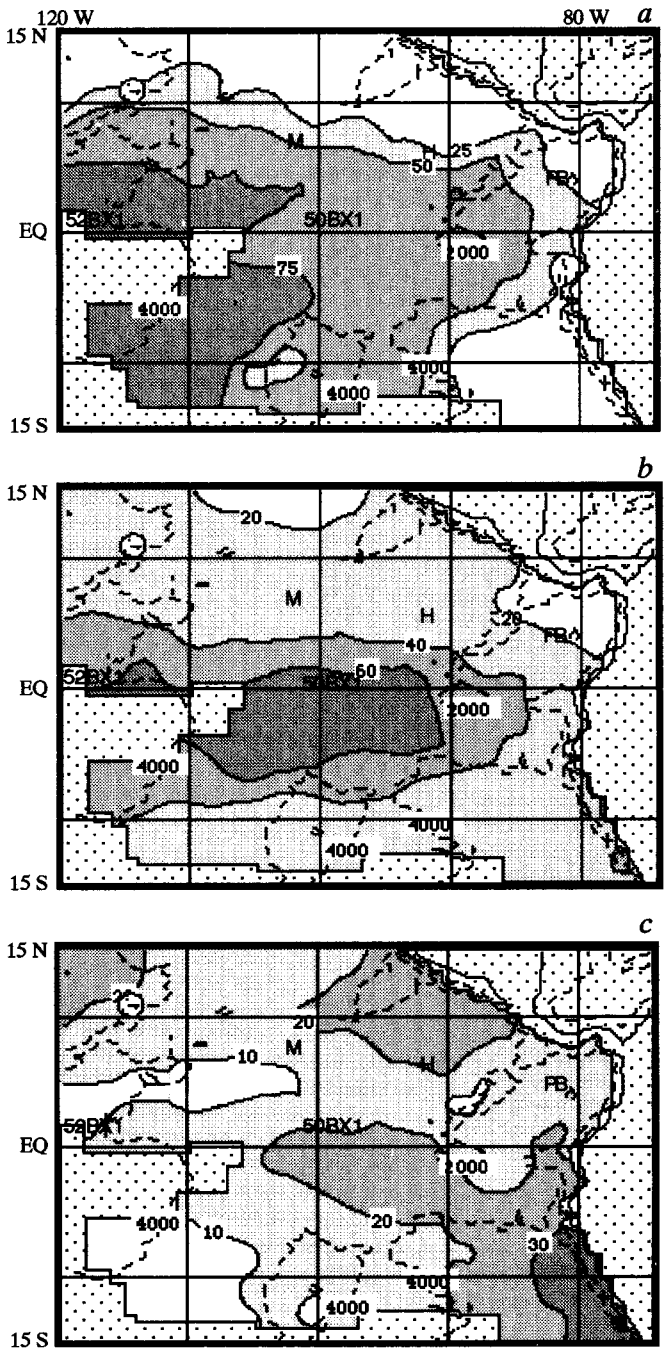

Fig. 5. Surface sediment characteristics in the Eastern Equatorial Pacific, from Lyle [1992]. Solid contours and shading indicate percentage dry weight, dashed contours indicate depth in meters, and areas of no data are stippled. (a) Percent calcite ($\%Cal_{tot}$), showing an equatorial maximum caused by high calcite productivity and a topographic high at the equator. (b) Percent opal, presented normalized to a calcite-free basis ($\%Opal_{calcite\text{-}free}$). The clear equatorial maximum has been interpreted as reflecting high opal productivity at the equator, but we argue that this may be an artifact of normalization. (c) Percent opal composition of total sediment ($\%Opal_{tot}$). $\%Opal_{tot}$ still exhibits some regional variability, but the clear equatorial maximum in $\%Opal_{calcite\text{-}free}$ is much diminished; values just as high as in the equatorial that can be found in the nearshore sediments and in the northern subtropics. Positions of sites listed in Table 1 are indicated.

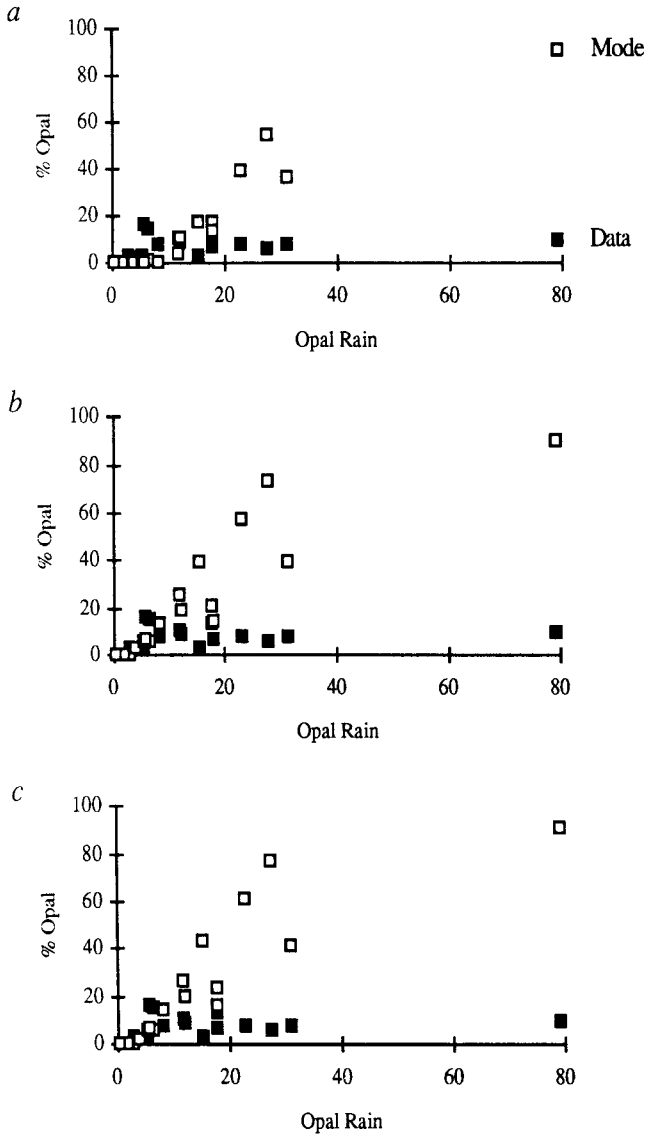

Fig. 6. $\%Opal_{tot}$ against opal rain (μmol cm^{-2} yr^{-1}), model (solid squares) versus data (open squares). (a) Homogeneous rain model. (b) Heterogeneous rain model (section 6). (c) Time dependent solubility model. Predictions from all three models greatly overestimate observations at high opal rain rates.

is extrapolated to higher opal rain, keeping all other parameters constant. MANOP site C curve B, where the opal rain is higher, is extrapolated to lower rain conditions. The squared dependence of the opal concentration on the rain rate is evident in the model results, until very high values of opal concentration are reached in curve A, at which point the simplifying assumption that burial is unimportant breaks down.

Further examination of equation (12) suggests a potential solution to the discrepancy between model results in the last section and data. In the pore water data set, we observed that the asymptotic Si concentration at 10-20 cm depth appeared to scale regionally with the rain rate of opal (Figure 3b). In equation (12), if the term Si_{sat} in the denominator is scaled to the rain rate of opal, rather than as a constant, then the solution to $\%Opal_{tot}$ scales as a constant (in the limit of high opal rain), rather than scaling with the rain rate squared, as before. Equation (12) also claims that knowing Si_{sat} is more crucial than knowing the dissolution kinetic rain constant, k_{op}, which only has a first-order effect on $\%Opal_{tot}$.

6. DIAGENESIS OF HETEROGENEOUS OPAL PHASES

Since the analysis in the previous section suggested that reproducing the observed pattern of asymptotic Si concentration may be crucial for reproducing $\%Opal_{tot}$, we search for a model for opal diagenesis that is able to reproduce the pore water observations. At this stage we limit our inquiry to hypotheses that assume that the "quality" of the sedimenting opal (i.e., solubility, kinetics, and fractional abundance of various phases) is independent of the magnitude of the opal rain rate. If this assumption proves tenable, then a predictive model for opal preservation may be possible.

Two alternative models of opal preservation seem like likely candidates for explaining the observed data, both involving multiple heterogeneous components of the sedimentary opal. In the first, the opal rain is divided into two components of differing solubility. In the second, the opal rain is homogeneous, but sedimentary opal transforms from one phase to another with some characteristic time scale. We show that either model is capable of generating the observed correlation between opal rain and asymptotic silica concentration, but that neither can account for the insensitivity of the observed $\%Opal_{tot}$ to opal rain. Both of the models rely on several parameters that are unconstrained by available data, so that the calculations merely demonstrate the feasibility of the proposed mechanisms to reproduce the pore water observations. Since burial represents only a small fraction of the opal rain for both of these models, the analysis presented in Section IV applies to these models as well as to the simpler, homogeneous opal model presented above.

Heterogeneous Rain Model

The heterogeneous rain model embodies the idea that the opal produced by organisms in the upper ocean may not be a homogeneous solid phase with a well-defined solubility, but may instead comprise a range of materials with a range of solubilities. It is well known that some species of diatoms are well preserved in sediments, while others, prominent in surface plankton assemblages, are completely removed from sediments by differential dissolution (for example, Shemesh et al. [1989]). Biogenic opal solubility is also known to be a function of cleaning [Lewin, 1961] and the aluminum content of the opal surface [Lewin, 1961; Willey, 1975; Iler, 1973].

We show results from the simplest configuration of the heterogeneous rain model, where the opal rain is represented as two phases. Each phase each phase is represented by an equation similar to equation (1a), and has a distinct solubility and dissolution rate constant. The concentration of dissolved silica is given by

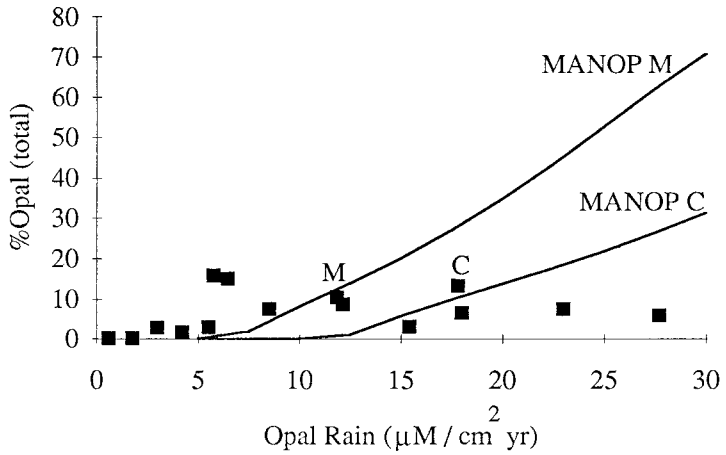

Fig. 7. Sedimentary opal concentration as a function of the opal rain rate, data compared with model results. Squares represent data from Table 1. Solid curves were generated by using MANOP sediment trap rain rates, and kinetics and solubility information inferred from pore water data at MANOP sites M and C, and varying the opal rain rate, with everything else held constant. Data from M and C from Table 1 are labeled "M" and "C." The model-predicted trend to higher opal concentration is not verified by the data.

$$\Phi \frac{\partial Si}{\partial t} = 0 = \frac{\partial}{\partial z}\left(\frac{D_{Si}}{F}\frac{\partial Si}{\partial z}\right) + k_{op}{}^{1}\ \%Op^{1}\ M_{op}{}^{-1} \cdot \rho\ \Phi\ (1-\Phi)\ (\ Si_{sat}{}^{1} - Si^{2+}\ )\ H(Si - Si_{sat}{}^{1}) + k_{op}{}^{2}\ \%Op^{2}\ M_{op}{}^{-1}\ \rho\ \Phi\ (1-\Phi) \cdot (\ Si_{sat}{}^{2} - Si\ )\ H(Si^{2+} - Si_{sat}{}^{2}) \quad (14)$$

where the superscripts 1 and 2 represent the rate constant, concentration, and solubility parameters of opal phases 1 and 2. The Heaviside function (H) inhibits precipitation of a supersaturated phase. This somewhat arbitrary assumption, along with, in this simplest case, five parameters that are unconstrained by the data (solubilities, rain composition, and rate constants), mean that this exercise merely demonstrates the feasibility of reproducing the observations with a mechanism of this type.

The behavior of the heterogeneous model asymptotic silica concentration and %Opal results is illustrated by Figure 8a and 8b. The two opal fractions differ only by their solubilities, with values of 1000 and 200 μmolar. The model was run using with fraction of the rain that is the more soluble component ranging from 0.1 to 0.9, in increments of 0.1. We see that the model asymptotic Si concentration scales linearly with the rain rate of opal, as observed, when 50% or less of the opal rain is the more soluble fraction. Under all conditions, however, the solid opal concentration increases with increasing opal rain. The model predicted opal concentrations for each location in Table 1 tend to overestimate the data at high opal rain rates (Figure 8b). Thus, for some range in parameter space, the model is able to reproduce the character of the pore water data, but not the observed concentrations of opal in the sediment.

Time-Dependent Solubility Model

The time-dependent solubility model represents the opal rain as a single homogeneous phase, which dissolves according to a well-defined solubility and rate constant. This phase also transforms into a second opal phase (perhaps simply by modification of its exposed surfaces) with a second set of kinetic parameters. Two separate, coupled solid diffusion / reaction equations similar to equation 1 are required to simulate the system. The reaction term for the raining component (analogous to expression 1a) is

$$R_{opal} = k_{op}{}^{1}\ \%Op^{1}\ M_{op}{}^{-1}\ \rho\ \Phi\ (1-\Phi)\ (Si_{sat}{}^{1} - Si) - K_{12}\ \%Op^{1}\ M_{op}{}^{-1}\ \rho\ (1-\Phi) \quad (15a)$$

where K_{12} is a first-order rate constant describing the solid transformation. The rate term for the second opal phase is

$$R_{opal} = k_{op}{}^{2}\ \%Op^{2}\ (Si_{sat}{}^{2} - Si) + K_{12}\ \%Op^{1}\ M_{op}{}^{-1}\ \rho\ (1-\Phi) \quad (15b)$$

Since the rain rate of the second opal phase is taken to be zero, the upper boundary condition for this phase is

$$(\ 1 - \Phi)\ D_B \left.\frac{\partial \%Op^{2}}{\partial z}\right|_{0} - w(0)\ \%Op^{2} = 0 \quad (15c)$$

The equation for dissolved silica is given by equation (14).

The results of a calculation of this type are presented in Figure 9. The two fractions of opal differ only by their solubilities, with values of 1000 and 200 μmolar, as before. The model was run with values of the "time constant", which controls the kinetics of solid transformation from the more soluble form to the less soluble ($1/K_{12}$ in equation 15a and b), ranging from 100 to 1000 years, in increments of 100 years. When $1/K_{12}$ is short relative to the characteristic mixing time of the sediment mixed layer ($\tau = (10\ cm)^2/0.150\ cm^2\ y^{-1} =$ 650 years), then the more soluble form is incompletely mixed to depth in the mixed layer, and the asymptotic Si value

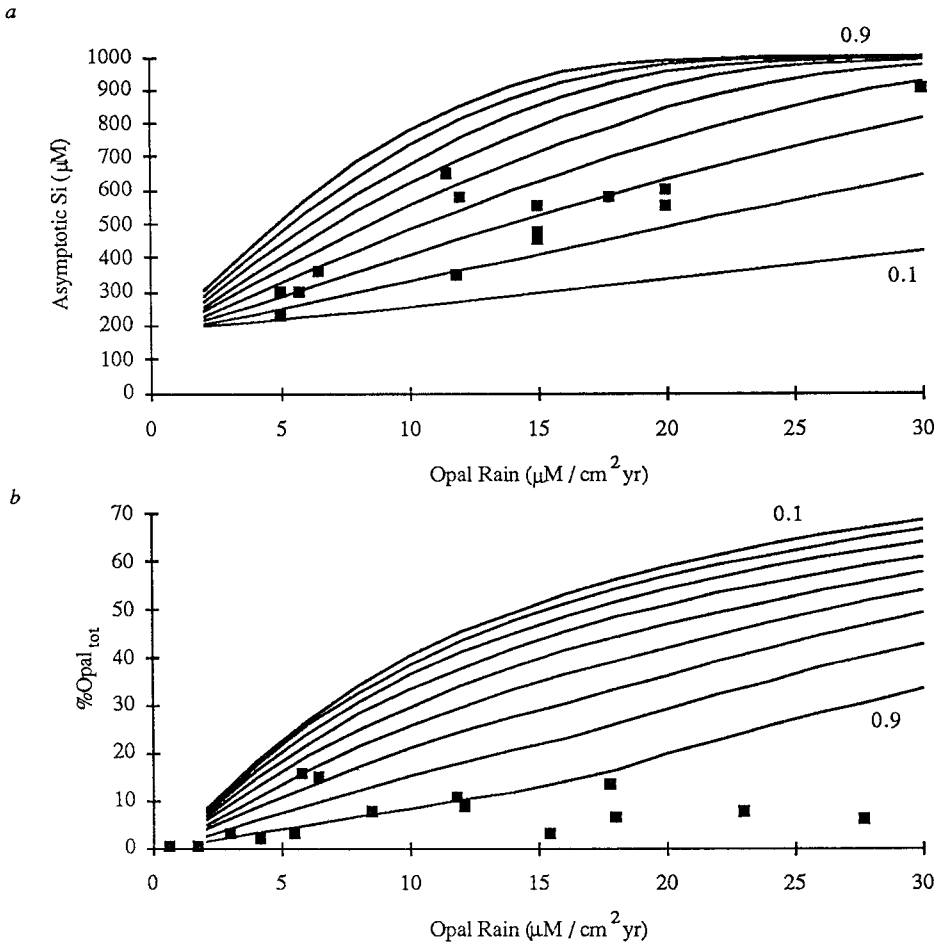

Fig. 8. Results from the "heterogeneous rain model". (a) Si concentration at 10 cm. (b) $\%Opal_{tot}$ (sum of both fractions). Data (from Figures 3 and 1c) are plotted squares. Rain rates of calcite and organic carbon were held constant at 18 and 12 μmol cm^{-2} yr^{-1}, respectively. Opal rain spanned 2-30 μmol cm^{-2} yr^{-1}. The opal rain comprised two fractions, with dissolution rate constants of 100 yr^{-1} for both, and solubilities of 1000 μM and 200 μM. Overlying water silica was 150 μM. The curves were generated using values of the fraction in the rain of the more soluble material ranging from 0.1 to 0.9 in increments of 0.1. The model is able to generate a roughly linear relationship between Si_{max} and opal rain, as observed in the data (a), but the model predicts an increase in %Opal with increasing opal rain, which is not observed (b).

increases linearly with opal rain. When K_{12} is long relative to mixing, then the asymptotic Si value saturates at the solubility of the more soluble form, for intermediate and high values of the opal rain. However, as for the heterogeneous opal rain model, this model predicts a clear increase in $\%Opal_{tot}$ with opal rain, again failing to reproduce the observed behavior of opal in sediments (Figure 7 (c)).

7. VARIATION OF OPAL "QUALITY" AS A FUNCTION OF OPAL PRODUCTION

We have failed to find a model for opal diagenesis that can take varying rain rates of opal of a constant "quality" (solubility, dissolution kinetics, etc.) and produce the observed pattern of opal preservation in the ocean. In desperation, we test the hypothesis that the opal rain is a single, homogeneous phase whose solubility is correlated with the rain rate of opal (a "scaled solubility" model). Guided by equation (12), we expect that this model will generate $\%Opal_{tot}$ that is nearly independent of the opal rain, as observed. In fact, this hypothesis does predict the observed patterns of both the asymptotic Si concentration and the $\%Opal_{tot}$ (Figure 10).

Variables that may correlate with opal production and could generate some systematic variation in opal solubility with production might be precipitation rate, temperature, or species assemblage. Unfortunately, mass quantitative estimates of radiolarian versus diatom fluxes in sediment traps are difficult to make, and are considered unreliable. The relative

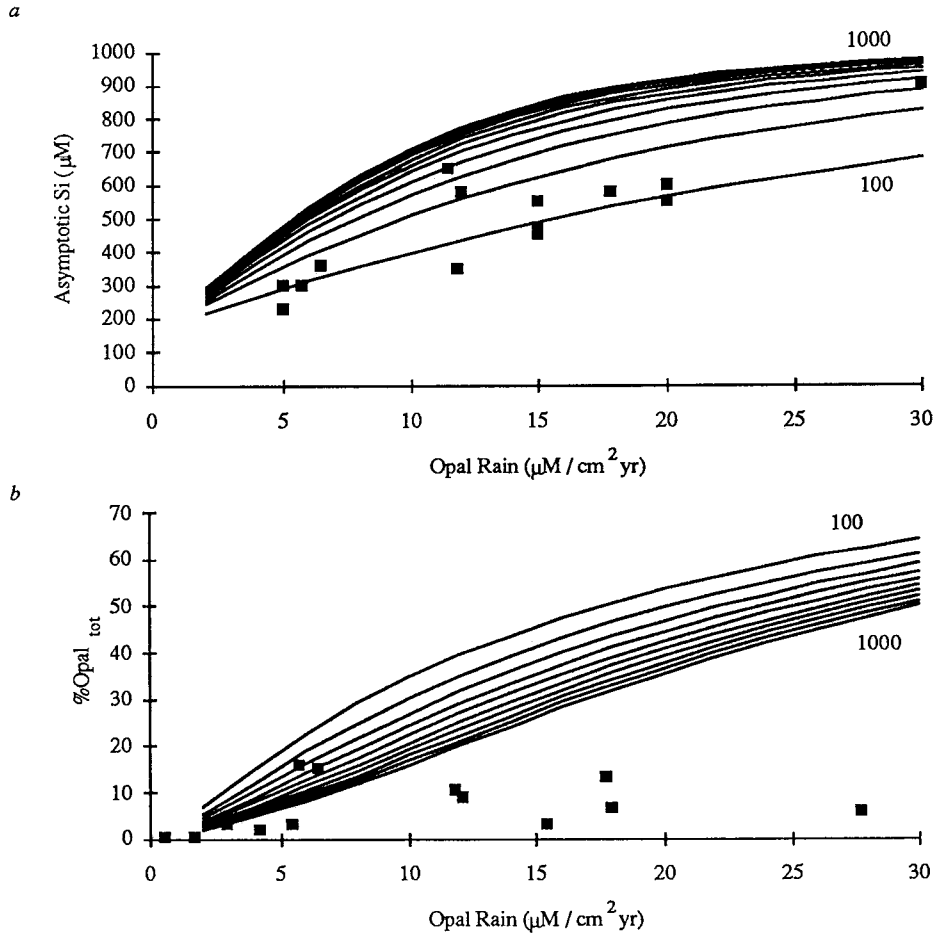

Fig. 9. Results from the "time dependent solubility" model. (a) Asymptotic pore water silica concentration, and (b) sediment solid opal content. Rain rates, solubilities, and dissolution kinetics of the opal phases are the same as for Figure 8. However, all of the raining material is the more soluble phase, which transforms into the less soluble phase with some time constant ranging from 100 to 1000 years, in increments of 100 years. When the time constant for solid transformation is fast relative to the mixing time of the sediment mixed layer, the model predicts a linear increase in pore water silica with increasing opal rain, as observed. However, the model predicts an increase in %Opal with increasing opal rain, that is not observed in the data.

solubilities of different types of undisturbed biogenic opal have not been adequately measured. Perhaps the concentration of silica in sediment trap collection cups could serve as an indicator of regional or temporal variations in bulk opal solubility.

One promising avenue of inquiry appears to be the effect of aluminum on opal solubility. Van Bennekom et al. [1991] observed a strong correlation of laboratory-determined biogenic opal solubility and the aluminum content of the opal. Van Bennekom et al. [1989] report high concentrations of opal (35-65%) in deep-sea sediments off the Zaire fan, characterized by high concentrations of Al substituted for opaline Si, and low interstitial pore water [Si] (250-370 μM). Laboratory measured solubilities of sediment samples were similar to the observed asymptotic pore water Si concentration. They concluded that the abundant supply of Al to the region (either to the upper ocean where opal is formed, as dissolved river effluent, or to the pore water by release from kaolinite and gibbsite) is responsible for the high Al concentrations in the opal, and that the decreased solubility of the resulting high Al opal protects it from dissolution. However, other reports show either no correlation between pore water aqueous alumina and silica concentrations [Caschetto and Wollast, 1979] or a positive covariation (the wrong direction for alumina inhibition of silica solubility) [Stoffyn-Egli, 1982]. In addition, the tight correlation between production and apparent opal solubility inferred from pore water data would imply some link between aluminum and opal supply, which is difficult to envision.

We conclude that the answer to what controls $\%Opal_{tot}$ in sediments must lie in some systematic variation of the quality or character of opal with opal productivity. Until we

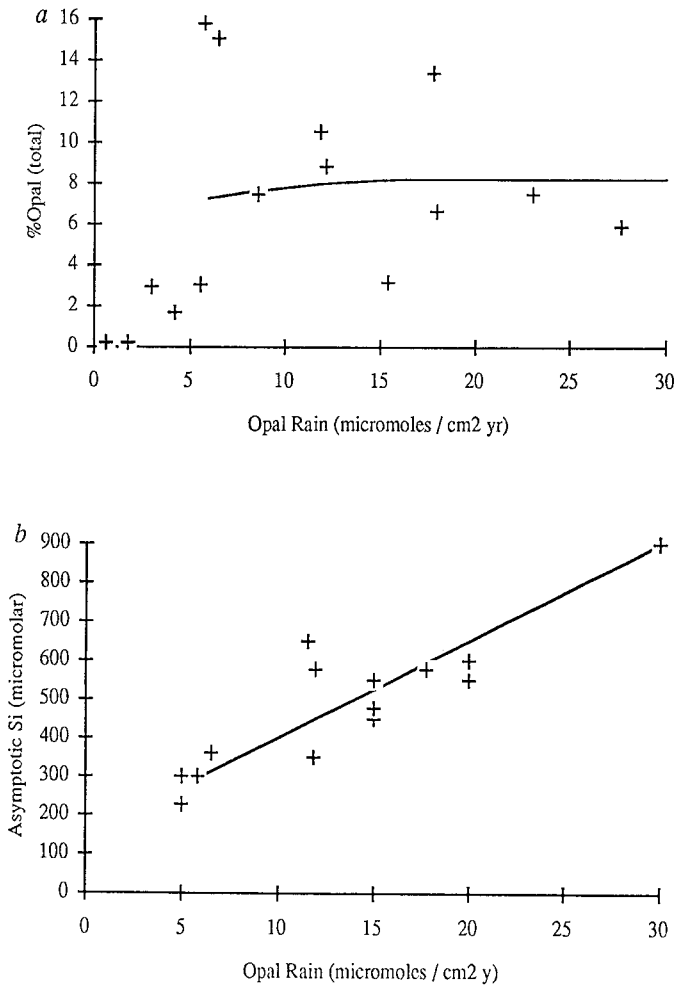

Fig. 10. Results from the "scaled solubility" model. Opal rain is represented as a single, homogeneous phase, but the solubility is taken to be a function of the opal rain, as $opal_{sat}(\mu M) = 150 + 25 * \text{opal rain } (\mu mol\ cm^{-2}\ yr^{-1})$. The model $\%Opal_{tot}$ is nearly independent of the rain rate, as observed.

understand more about what controls opal preservation in sediments today, we will be unable to interpret variations in opal preservations in the past.

SUMMARY

Using a numerical model for sediment diagenesis, and a compilation of data from sediments in the deep sea, we attempt to understand the factors that control the preservation of opal in sediments. The numerical model simulates the reaction, mixing, and burial of opal, calcite, organic carbon, and clay in the sediment mixed layer. In order to predict reaction rates, the model must also predict the chemistry within the diffusive medium of the pore water.

Our analysis suggests that the common practice of presenting and interpreting opal data on a "calcite free" normalized basis may introduce a calcite artifact into the opal data. This is because, when burial represents only a small fraction of the opal rain (as is the case in tropical sediments), the rain of opal must be balanced by dissolution, which is controlled by the concentration of opal as a fraction of the total, not calcite free, sediment. This effect may be responsible for the well-known maximum of $\%Opal_{calcite\text{-}free}$ in equatorial Pacific sediments, which is generally attributed to a high rain rate of opal in that region. The accumulation rate of opal across the model calcite lysocline appears to be closely tied to the burial rate of calcite. Thus we argue that opal MAR is also an unreliable indicator of opal production.

Two salient observations are made from the sedimentary data set. First, the asymptotic concentration of silica in the pore water correlates tightly with the rain rate of opal. Second, $\%Opal_{tot}$ appears to have little or no reliable trend with increasing opal rain. The simplest model for opal diagenesis, a homogeneous rain model, predicts that the asymptotic silica concentration should be nearly constant with opal rain, and that the opal concentration should scale with the opal rain squared. That is, the model clearly fails to reproduce both of the observations. We propose two more complex models of opal diagenesis, and show that either can reproduce the behavior of the pore water data, but neither can reproduce the constant $\%Opal_{tot}$ against opal rain observed in the data.

The factors that control the concentration of opal in real sediments must lie outside the scope of the model, such as regional variations in the solubility or dissolution kinetics of opal raining to the seafloor. We conclude that the interpretation of downcore opal concentration, either on a calcite free or a total sediment basis, simply in terms of changes in opal production, is not supported by our analysis. Until the factors that control opal preservation in today's ocean can be elucidated, it will be impossible to interpret patterns of opal preservation from the past.

Acknowledgements. This paper benefited from discussions with Wally Broecker, and comments by Robin Keir, David DeMaster, and Bernard Boudreau, and was supported by the Lamont Doherty Geological Observatory, the G. Unger Vettersen Foundation, and selected member companies of the International Petroleum Industry Environmental Conservation Association. This is LDEO contribution number 5038.

REFERENCES

Archer, D. E., The dissolution of calcite in deep-sea sediments: An in situ microelectrode study, pp., Ph.D. thesis, Univ. of Wash., Seattle, 1990.

Archer, D. E., Modeling the calcite lysocline, J. Geophys. Res., 96, 17,037-17,050, 1991.

Archer, D. E., and A. Devol, Benthic oxygen fluxes on the Washington shelf and slope: A comparison of in situ microelectrode and chamber flux measurements, Limnol. Oceanogr., 37, 614-629, 1992.

Archer, D., S. Emerson, and C. Reimers, Dissolution of calcite in deep-sea sediments: pH and O_2 microelectrode results, Geochim. Cosmochim. Acta, 53, 2831-2846, 1989.

Boudreau, B. P., Asymptotic forms and solutions of the model for silica-opal diagenesis in bioturbated sediments, J. Geophys. Res., 95, 7367-7381, 1990.

Boudreau, B. P., and J.T. Westrich, The dependence of bacterial sulfate reduction on sulfate concentration in marine sediments, Geochim. Cosmochim. Acta, 48, 2503-2516, 1984.

Broecker, W. S., and T. H. Peng, Tracers in the Sea. 689 pp., Eldigio Press, Palisades, N. Y., 1982.

Caschetto, S., and R. Wollast, Dissolved aluminum in interstitial waters of recent marine sediments, Geochim. Cosmochim. Acta, 43, 425-428, 1979.

Dymond, J., and M. Lyle, Particle fluxes in the ocean and implications for sources and preservation of ocean sediments, in Global Surficial Flux Study, edited by W. Hey and T. Usselman, National Academy of Sciences, Washington, D.C., in press, 1993.

Emerson, S., Organic carbon preservation in marine sediments, in The Carbon Cycle and Atmospheric CO2: Natural Variations Archean to Present, Geophys. Monogr. Ser, vol 32, edited by E.T. Sundquist and W.S. Broecker, pp. 78-87, AGU, Washington D. C., 1985.

Emerson, S., and M. L. Bender, Carbon fluxes at the sediment-water interface of the deep sea: Calcium carbonate preservation, J. Mar. Res., 39, 139-162, 1981.

Emerson, S., R. Jahnke, M. Bender, P. Froelich, G. Klinkhammer, C. Bowser, and G. Setlock, Early diagenesis in sediments from the Eastern Equatorial Pacific, I, Pore water nutrient and carbonate results, Earth Planet. Sci. Lett., 49, 57-80, 1980.

Fanning, K. A., and M. E. Q. Pilson, Interstitial silica and pH in marine sediments: Some effects of sampling procedures, Science, 17, 1228, 1971.

Fischer, G., D. Futterer, R. Gersonde, S. Honjo, D. Ostermann, and G. Wefer, Seasonal variability of particle flux in the Weddell Sea and its relation to ice cover, Nature, 335(6189), 426-428, 1988.

Honjo, S., S. J. Manganini, and J. J. Cole, Sedimentation of biogenic matter in the deep ocean, Deep Sea Res. 29, 609-625, 1982.

Honjo, S., Particle fluxes and modern sedimentation in the polar oceans, in Polar Oceanography: Part B: Chemistry, Biology, and Geology, edited by W. O. Smith, pp. 687-739, Academic, San Diego, Calif., 1990.

Hurd, D. C., Interactions of biogenic opal, sediment and sea water in the Central Equatorial Pacific., Geochim. Cosmochim. Acta. 37, 2257-2282, 1973.

Hurd, D. C., and F. Theyer, Changes in the physical and chemical properties of biogenic silica from the central equatorial Pacific; I, Solubility, specific surface area, and solution rate constants of acid-cleaned samples, in Analytical Methods in Oceanography, edited by T. R. P. Gibb, Jr., American Chemical Society, Washington, D. C., 1975.

Iler, R. K., Effect of adsorbed alumina on the solubility of amorphous silica in water, J. Colloid. Interface Sci., 43, 399-408, 1973.

Jahnke, R., D. Heggie, S. Emerson, and V. Grundmanis, Pore waters of the central Pacific Ocean: Nutrient results, Earth Planet. Sci. Lett., 62, 233-256, 1982.

Keir, R. S., The dissolution kinetics of biogenic calcium carbonates in sea water, Geochim. Cosmochim. Acta, 44, 241-252, 1980.

Lewin, J. C., The dissolution of silica from diatom walls, Geochim. Cosmochim. Acta, 21, 182-198, 1961.

Lyle, M., D. W. Murray, B. P. Finney, J. Dymond, J. M. Robbins, and K. Brooksforce, The record of late pleistocene biogenic sedimentation in the Eastern Tropical Pacific Ocean, Paleoceangraphy, 3, 39-59, 1988.

Lyle, M., Composition maps of surface sediments of the eastern tropical Pacific Ocean, in Proc. O.D.P. Init. Reports, Leg 138, edited by L. Mayer, N. Pisias, T. Janetek et al., pp 101-119, Ocean Drilling Program, College Station, TX, 1992.

Martin, W. R., M. Bender, M. Leinen, and J. Orchardo, Benthic organic carbon degradation and biogenic silica dissolution in the central Equatorial Pacific, Deep Sea Res., 38, 1517-1530, 1991.

Murray, J. W., and V. Grundmanis, Oxygen consumption in pelagic marine sediments, Science, 209, 1527-1530, 1980.

Rea, D. K., N. G. Pisias, and T. Newberry, Late Pleistocene paleoclimatology of the central equatorial Pacific: Flux patterns of biogenic sediments, Paleoceangraphy, 6, 6227-244, 1991.

Schink, D. R., K. A. Fanning, and M. E. Q. Pilson, Dissolved silica in the upper pore waters of the Atlantic Ocean floor, J. Geophys. Res., 79, 2243-2250, 1974.

Schink, D. R., N. L. J. Guinasso, and K. A. Fanning, Factors affecting the concentration of silica at the sediment-water interface of the Atlantic ocean, J. Geophys. Res., 80, 3013, 1975.

Shemesh, A., L. H. Burckle, and P. N. Froelich, Dissolution and preservation of Antarctic diatoms and the effect on sediment Thanatocoenoses, Quat. Res., 31, 288-308, 1989.

Stoffyn-Egli, P., Dissolved aluminum in interstitial waters of recent terrigenous maring sediments from the North Atlantic Ocean, Geochim. Cosmochim. Acta, 46, 1345-1352, 1982.

Ullman, W., and R. C. Aller, Diffusion coefficients in near shore marine sediments, Limnol. Oceanogr., 27, 552-555, 1982.

van Bennekom, A., J. Jansen, S. v. d. Gaast, J. v. Iperen, and J. Pieters, Aluminum-rich opal: An intermediate in the preservation of biogenic silica in the Zaire (Congo) deep-sea fan, Deep Sea Res., 36, 173-190, 1989.

van Bennekom, A. J., A. G. J. Buma, and R. F. Nolting, Dissolved aluminum in the Weddell-Scotia confluence and effect of Al on the dissolution kinetics of biogenic silica, Mar. Chem., 35, 423-434, 1991.

Willey, J. D., Silica - alumina interactions in sea water, Mar. Chem., 3, 241-251, 1975.

D. Archer, P. Froelich, and K. Rogers, Lamont-Doherty Earth Observatory, Palisades, NY 10964.

M. Lyle, Department of Geosciences, Boise State University, Boise, ID 83725.

(Received August 4, 1992;
revised November 23, 1992;
accepted November 28, 1992)